THE JOURNAL OF PHYSICAL CHEMISTRY A

Article

pubs.acs.org/JPCA

Capture of Hyperthermal CO_2 by Amorphous Water Ice *via* Molecular Embedding

Grant G. Langlois,[†] Wenxin Li,[†] K. D. Gibson, and S. J. Sibener*

The James Franck Institute and Department of Chemistry, The University of Chicago, 929 E. 57th Street, Chicago, Illinois 60637, United States

ABSTRACT: We present the first study detailing the capture and aggregation of hyperthermal CO_2 molecules by amorphous solid water (ASW) under ultra-high vacuum conditions at 125 K, near the amorphous/crystalline transition. Using time-resolved *in situ* reflection−absorption infrared spectroscopy (RAIRS), CO_2 molecules with translational energies above 3.0 eV are observed to directly embed underneath the vacuum−solid interface to become absorbed within the ice films despite an inability to adsorb at 125 K; this behavior is not observed for crystalline films. Upon embedding, the mobility of CO_2 within 125 K amorphous ice and the strength of its intermolecular interactions result in its segregation into clusters within the ice films. Tracing the kinetics of CO_2 embedding events under different energetic conditions allows for elucidation of the underlying dynamics, and we draw comparison with other projectiles we have studied to promote generalized conclusions in regard to empirical prediction of a projectile's embedding probability. Through application of a classical model of the entrance barrier for projectiles colliding with amorphous ice, we provide direct evidence for a unified connection between embedding probability and projectile momentum; an account of all embedding data measured by our group traces a unified barrier model. This work highlights the interplay between translational energy and momentum accommodation during collisions with ice in high speed gas flows.

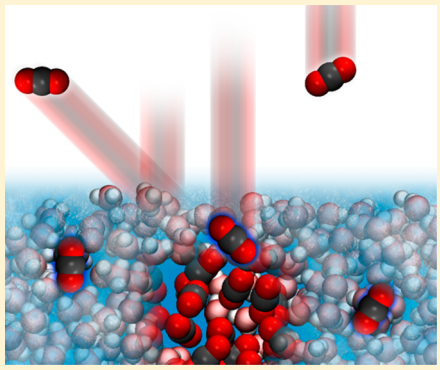

■ INTRODUCTION

The interaction of gases with ice is fundamental to numerous scientific disciplines. In astrophysics, theories of atmospheric formation on planets and moons focus primarily on delivery of volatile species from comets.[1−4] Simple gaseous species accumulate and concentrate within the ices of comets and pre-cometary matter,[5,6] potentially subject to bombardment by high-energy electromagnetic radiation and interstellar matter to form complicated molecules.[7] Simulation of these processes in many laboratories using pre-mixed cometary ice analogs has produced organic residues containing molecules potentially important in understanding possible sources of prebiotic chemistry on Earth.[8−14] Additionally, answers to important questions related to geophysics and global energy issues are built upon the foundation of a thorough understanding of gas−ice interactions, with intense focus on clathrate hydrates,[15,16] whose contemporary applications include endeavors into hydrogen storage[17,18] and capture of anthropogenic greenhouse gases.[19,20]

CO_2, along with its interaction with ice, represents a major constituent of interstellar matter[21,22] and is hypothesized to be a major component of global climate forcing. Comparison between the sequestration and release of CO_2 by glacial ice during prior geological epochs and the current global climate provides tangible links to consequences associated with Earth's currently melting permafrost.[23,24] In this work, we present the first study on the capture and concentration of neutral, hyperthermal CO_2 by amorphous solid water (ASW) under ultra-high vacuum (UHV) conditions at a surface temperature where CO_2 adsorption is infeasible as a method of accretion. We demonstrate that the observed CO_2 uptake by ASW at 125 K is dominated by the process of energetic ballistic deposition, or "embedding". This is a phenomenon we have described at length in previous publications, whereby small atoms and molecules with high translational energies and trajectories near normal incidence directly bury underneath the vacuum−solid interface upon collision.[25−28]

Finally, we draw comparisons between the observed embedding efficacy of CO_2 in amorphous water ice and the other gaseous projectiles studied by our group (Xe, Kr, CF_4, SF_6) and via application of a classical empirical model to the activated process, firmly establish a generalized connection between projectile momentum and embedding probability.

The embedding of CO_2 and other small atoms and molecules into ASW inherently differs from percolation into the bulk following adsorption onto an icy surface, which itself is well characterized.[5,6,29−33] Namely, our results imply that ice composition can be modified by gases with high translational energies, even when ice temperature precludes adsorption.[7,8]

Special Issue: Dynamics of Molecular Collisions XXV: Fifty Years of Chemical Reaction Dynamics

Received: June 30, 2015
Revised: August 1, 2015
Published: August 14, 2015

DOI: 10.1021/acs.jpca.5b06287
J. Phys. Chem. A 2015, 119, 12238−12244

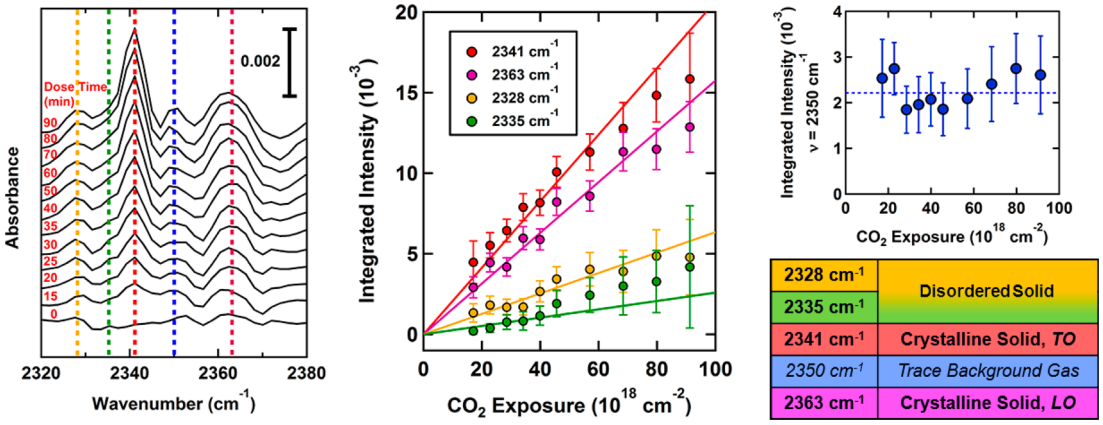

Figure 1. Representative RAIR spectra obtained during exposure of 4.1 eV CO_2 to 60-layer-thick amorphous H_2O ice film. Boldface signals in the table (2328, 2335, 2341, 2363 cm^{-1}) are associated with solid CO_2 uptake, whose integrated peaks grow linearly as a function of total exposed CO_2. The signal at 2350 cm^{-1} is associated with trace background CO_2 in the IR beam path within the sample chamber and remains essentially constant throughout the experiment, as shown in the top-right plot.

These findings have direct implications in studies of planetesimals traveling at high speeds in protoplanetary nebulae,[34] and in studies and simulations of the hazardous icing of aircraft during flight.[35,36]

■ EXPERIMENTAL DETAILS

The experiments referenced herein were conducted in a molecular beam scattering instrument described at length in a previous publication.[37] The instrument consists of a triply differentially pumped supersonic molecular beam connected to an ultra-high vacuum (UHV) chamber equipped, in part, with optics for performing time-resolved reflection−absorption infrared spectroscopy (RAIRS).

Ice coverage and CO_2 uptake in all experiments were quantified by integrating RAIR spectra by fitting observed bands with Gaussian peaks atop cubic baselines. All spectra were obtained using a Nicolet model 6700 infrared spectrometer with incident *p*-polarized IR radiation reflected from the underlying Au(111) crystal at an incident angle of 75° and directed into a liquid-nitrogen-cooled MCT/A detector. Spectra were averaged over 250 scans taken at 4 cm^{-1} resolution with clean Au(111) as background. A total of 60−75 layers (one layer = 1.07×10^{15} H_2O molecules[38,39]) of low density amorphous ice were deposited onto single-crystal Au(111) at 125 K, promoting both substrate independence and homogeneity, i.e., self-similar structural presentation for layers of this thickness, at the vacuum−solid interface.[39,40] Under these conditions, the sticking coefficient of H_2O on both Au and ice is nearly unity,[37] and H_2O desorption is negligible over a period of hours. Ice thickness was quantified by backfilling the main chamber at a known deposition rate with respect to the Au(111) surface and correlating the rate with growth of the integrated intensity of the ∼3300 cm^{-1} OH band.[41] This quantitation is valid with ice film thicknesses up to 200 layers using our setup, after which the OH band shape changes significantly due to a change in optical field penetration.

To produce the highest possible CO_2 translational energies in our beam, we expand ∼1% CO_2 diluted in H_2 at 400−600 psi through a 15 μm molybdenum pinhole, with all exposure to ice at normal incidence. CO_2 translational kinetic energies ranging from 0.9 to 4.1 eV are obtainable by resistively heating the beam nozzle from room temperature to 1200 K, with energy distribution widths ($\Delta E/E$) ranging from 18 to 46% depending upon nozzle temperature and pressure, as characterized using time-of-flight techniques. We note that this method of producing CO_2 with high translational energies causes CO_2 and H_2 to readily react under some of the chosen conditions, to near completion as the nozzle temperature approaches 1200 K at all stagnation pressures used, producing CO and H_2O through the reverse water−gas shift reaction[42] either homogeneously or catalytically by the exposed metal surfaces. Similar beam reactivity phenomena were reported by Herschbach et al. in the case of small hydrocarbons forming larger hydrocarbons within the nozzle of a molecular beam under analogous conditions.[43] We plan to present the specifics of these interesting findings in an upcoming publication. Though no evidence of CO accumulation is observed on or within the ice surfaces discussed in this paper, H_2O is deposited throughout our experiments with a rate typically at or below $\sim 10^{-2}$ layers per second as a product of the reverse water−gas shift reaction taking place.

Total CO_2 flux from the seeded molecular beams is determined by first calibrating the pressure rise in the sample chamber with a nude Bayard−Alpert ion gauge while open to neat CO_2 beams.[28] With knowledge of the chamber pumping speed, the relative sensitivity of the gauge to CO_2,[44,45] and the beam's spot size on the Au(111) crystal, the molecular flux of the neat beam is determinable. For neat beams at different stagnation pressures, the calculated fluxes were each correlated with an observed rise in signal at m/z = 44 when open to the chamber as measured by a residual gas analyzer (RGA) located outside of the beam's line of sight. Linear regression yields direct conversion between RGA signal rise and total CO_2 flux, and in this way, CO_2 flux in seeded beams could be determined purely from the RGA readings for all experiments.

■ RESULTS AND DISCUSSION

Embedding: Ice Structure and Composition. Upon exposure of ASW to high-translational-energy CO_2, a rich profile of local environments are observed between 2320 and 2380 cm^{-1}. Figure 1 depicts example chronological spectra obtained by continuously exposing an ASW film to CO_2 with average translational energy of 4.1 eV. Although our analysis focuses primarily on monitoring the intensity of the most prominent mode at 2341 cm^{-1} as a function of exposure and CO_2 translational kinetic energy, the overall IR response of the

DOI: 10.1021/acs.jpca.5b06287
J. Phys. Chem. A 2015, 119, 12238−12244

film encompasses detailed information about the structure of the ice film after embedding and is worth highlighting. The sharp (fwhm < 5 cm^{-1}) signal at 2341 cm^{-1} exhibits a 4 cm^{-1} red shift compared to signals observed in pure CO_2 ices, both thick and thin.[33,46,47] This observation aligns with those made in several studies; CO_2 weakly interacting with surrounding water decreases the ν_3 mode's effective force constant, making a distinction between *surface adsorbed* and *bulk absorbed* CO_2 trivial.[47,48] Given that stable CO_2 deposition occurs below 90 K[32] (much lower than our experimental conditions) and that another signal does not appear near 2345 cm^{-1}, we infer that all CO_2 accumulated on the surface must be buried beneath the vacuum−solid interface, despite the fact that the ASW film is nonporous as prepared.[49] It is also important to note that we do not observe uptake when the ice film is crystalline. This observation is consistent with our prior reports of embedding and persistence occurring more readily within amorphous films, compared to crystalline films; molecular dynamics simulations of hyperthermal Xe collisions with crystalline ice produce trajectories whereby a Xe atom is ejected from within the selvedge on the order of picoseconds.[25−28]

Concurrent with growth of the 2341 cm^{-1} peak is growth of a peak at 2363 cm^{-1}, suggesting that accumulated CO_2 molecules are not homogeneously, "infinitely" diluted within the ice but concentrated into small aggregates. This is in agreement with one study concluding that CO_2 is mobile within ice above 60 K and exhibits a high degree of segregation when deposited above this temperature; CO_2 exists within ices of this nature mostly as pure crystallites.[50] This peak assignment further aligns with numerous studies of CO_2 clusters in both pure gaseous and solid phases.[51−55] The two aforementioned peaks correspond, respectively, to the transverse optical (TO) and longitudinal optical (LO) modes of the crystallites, and the peak position of the LO mode in particular (2363 cm^{-1}) suggests that CO_2 aggregates within the ice resemble rods, as opposed to large slabs (2381 cm^{-1}) or spheres (2356 cm^{-1}).[56−58] Offering insightful contrast, CF_4 showed no signs of clustering after embedding into ASW grown under identical conditions in our prior work.[28] Aggregation dynamics within the ice film are expected to depend on both the mobility of the absorbed species and the relative energetic interactions between guest and host molecules. CF_4 molecules are quite similar to noble gases in terms of their intermolecular interactions; high symmetry and small size leads to CF_4's weak electrostatic interactions with itself and other molecules.[59] Interaction energies of CF_4 with itself and water are each on the order of only a few kJ/mol,[60−62] whereas CO_2 dimer interaction energy is roughly equal to, if not greater than, that of CO_2−H_2O, and closer in magnitude (∼20−25 kJ/mol) to the H_2O dimer interaction energy (∼40 kJ/mol).[32,63]

Aside from an unchanging weak absorption at 2050 cm^{-1} from trace gaseous CO_2 in the IR beam path, Figure 1 also tracks two weak features at 2328 and 2335 cm^{-1}. The former has previously been identified in literature as belonging to amorphous or disordered CO_2,[64] although our surface is well above the temperature at which amorphous CO_2 is stable. Indeed, extremely red-shifted spectral features have been reported in CO_2/H_2O mixtures,[65] but again, studies such as these were conducted at temperatures well below 125 K, complicating direct comparison. Literature studies suggest that, for instance, the surface and subsurface layers of water ice nanocrystals can have differing degrees of disorder compared to their cores,[66,67] and absent any confirmation by high-level theoretical simulations of this system, it remains plausible that CO_2 aggregates formed after embedding exhibit analogous behavior.

Kinetics and Dynamics of CO_2 Embedding in Ice. As noted in the Experimental Details, H_2O can also be generated in the seeded supersonic molecular beam at the nozzle temperatures required to obtain CO_2 with the highest translational energies studied. Consequently, H_2O is also deposited onto the ice film throughout CO_2 exposure, typically at or below a rate of ∼10^{-2} layers per second. To deconvolute our observations from this codeposition, and to confirm no modification of our embedding results due to the presence of low water flux, a series of control experiments were executed, with results detailed in Figure 2. Ice films were either exposed

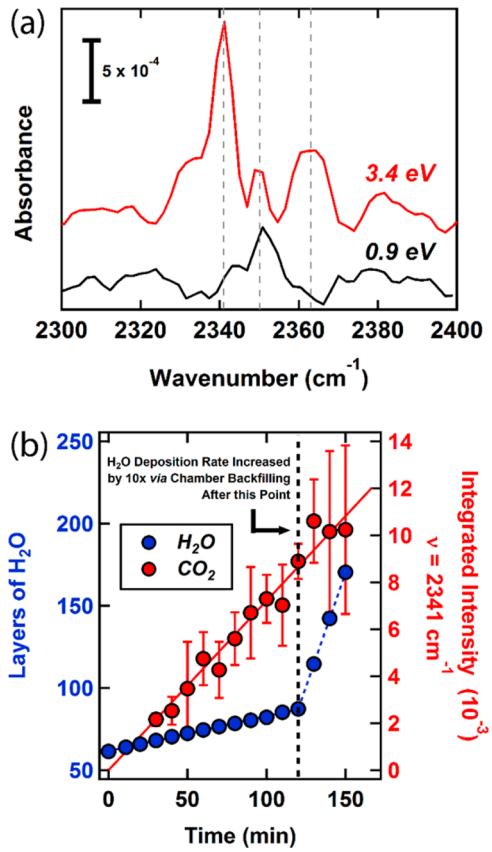

Figure 2. (a) CO_2 RAIRS signals obtained during exposure to a high-translational-energy seeded CO_2 beam (red) and during low-translational-energy beam codeposition of CO_2/H_2O (black). High CO_2 translational energies are required for resolution of solid CO_2 spectroscopic signals. (b) Embedding experiment with two different total H_2O deposition rates over the course of exposure, showing no change in the rate of CO_2 uptake as measured by RAIRS and demonstrating the observed accumulation's independence from background water deposition.

to CO_2/H_2O mixtures (produced by bubbling CO_2 through an H_2O filled reservoir) or exposed to a lower energy (∼1 eV) CO_2 beam during simultaneous backfilling of the sample chamber with pure water vapor. Figure 2a compares RAIR spectra from both high- and low-energy trials with equal total CO_2 exposures. In all cases, only trace gaseous background CO_2 (2050 cm^{-1}) was observed when low-energy CO_2 was used, irrespective of the total H_2O codeposition rate and the manner in which H_2O was deposited. Figure 2b shows an

DOI: 10.1021/acs.jpca.5b06287
J. Phys. Chem. A 2015, 119, 12238−12244

embedding experiment where, beginning at the 120 min mark, the total deposition rate of H_2O was deliberately increased by 1 order of magnitude via simultaneous backfilling of the chamber with H_2O. As evidenced by the plot, the CO_2 uptake rate remains constant despite the large differences in H_2O deposition rate. Thus, these results confirm the embedding rate's independence from the low water flux; burying does not occur. These findings are, again, further backed by temperature-programmed desorption (TPD) experiments in the literature performed on both Au(111) and H_2O ice that place stable deposition of CO_2 at surface temperatures well below 125 K.[32]

The initial CO_2 uptake rate is observed to be linear with respect to the amount dosed in all measurements made with exposure to CO_2 with translational energy 3.0 eV or greater. Figure 3 shows uptake rates of CO_2 by amorphous ice at three

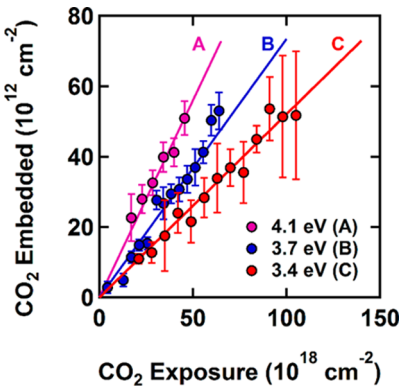

Figure 3. Initial embedding probabilities on ASW for three different average CO_2 energies. See text for details regarding conversion of ordinate axes from integrated peak intensity to number embedded. Over the energy range studied, as the average kinetic energy of the incident CO_2 increases, the initial embedding probability also increases.

different average translational energies with the abscissae of each data set normalized to each other via multiplication of the total exposure time to the beam at each time point by the experiment's respective CO_2 flux. To approximate the total amount of CO_2 molecules embedded at any given time, the integrated intensity of the 2341 cm^{-1} peak is divided by the absorptivity of this mode for CO_2 diluted in ice (1:10), as measured via transmission IR by Sandford and Allamandola at 10 K.[63] The absorptivity is linearly corrected to one at 125 K, as discussed in their paper. Given this transformation, the slopes of the linear uptake curves represent initial embedding probabilities for CO_2 at the respective energetic conditions. As seen in Figure 3, the initial uptake rate is clearly highest for the most energetic CO_2 molecules.

The CO_2 molecules in the molecular beam populate a translational energy distribution with a finite width, and therefore each embedding probability measured represents a convolution of the energy distribution with a small range of probabilities. To deconvolute the data and extract the true energy dependence outlining the dynamics of the embedding process, a polynomial nonlinear least-squares fit to the data, $f(E)$, was employed as an ansatz for the actual rate dependence and deconvoluted from the incident energy distribution, $P(E)$, to give the measured dependence, $F(E)$, as plotted in Figure 4a:

$$F(E) = \int f(E)\, P(E)\, \mathrm{d}E \tag{1}$$

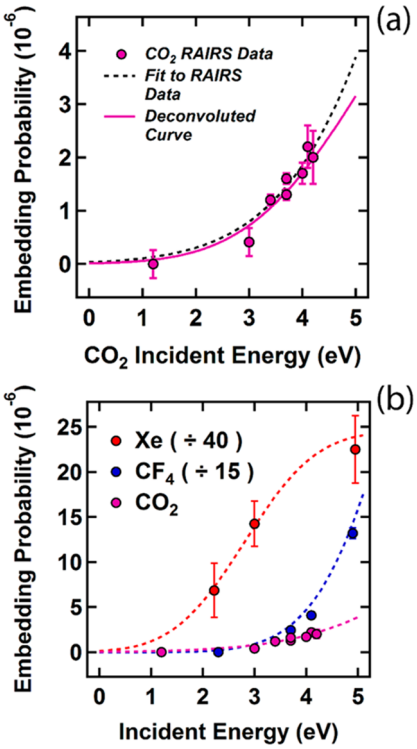

Figure 4. (a) Initial CO_2 embedding probability increasing as a function of incident kinetic energy. Measured data are deconvoluted from the CO_2 energy distributions using a polynomial ansatz, yielding the solid purple curve (see text for details). (b) Application of constrained, parameterized *S*-curves to the data allowing for comparison of CO_2 embedding probabilities to those previously measured for CF_4 and Xe. Over a similar energy range, the embedding probability for CO_2 is measured to be smaller by roughly 1 and 3 orders of magnitude as compared to CF_4 and Xe, respectively.

The results are consistent with conclusions made previously, namely, that (a) there is a rapid increase in embedding probability above some energetic threshold, and (b) given that the projectile is below a critical size, the mass of the projectile is important in predicting embedding efficacy.[28] Figure 4b clarifies this point, revealing the embedding probability of ~4 eV CO_2 to be roughly 1 and 3 orders of magnitude lower than that of homo-energetic CF_4 and Xe, respectively, despite all three projectiles having similar sizes (radii as estimated from gas-phase van der Waals *b* parameters:[68] CO_2, 2.1 Å; CF_4, 2.9 Å; Xe, 2.7 Å).

Embedding as an Activated Process. For a projectile to embed, it clearly must first overcome an energetic barrier associated with traveling beyond the immediate vacuum−solid interface to become buried within or underneath the selvedge, and therefore embedding can be considered an activated process. As originally established by Lennard-Jones, the paradigmatic notion of a barrier formed from the crossing of repulsive and attractive states between a gaseous projectile and a metal surface sought to describe the dynamics of dissociative adsorption.[69] The underlying dynamics behind projectiles embedding into ASW draw close comparison with these processes upon inspection (e.g., rapid increase above a threshold, saturation at high energy), and application of an empirical classical barrier to this entrance channel offers an opportunity to draw useful conclusions by comparing the dynamics of all projectiles we have studied, including CO_2. To this end, we adopt an *S*-shaped, parameterized form for the

DOI: 10.1021/acs.jpca.5b06287
J. Phys. Chem. A 2015, 119, 12238−12244

embedding probability used to evaluate the dissociative adsorption dynamics of molecular hydrogen on single-crystal copper surfaces[70] and described by Harris:[71]

$$\sigma(E) = \frac{A}{2}\left(1 + \tanh\frac{E - E_0}{W}\right) \quad (2)$$

In the above equation, E_0 represents the energetic barrier, W represents the range of energies over which the curve rises (related to a distribution of barrier heights dependent upon position of impact), and A represents the saturation value for the probability.

The application of this empirical model to our data is presented in Figure 4b. We expect that ice morphology critically influences the embedding process (projectiles are more deeply embedded in amorphous ice[25−28]), and although the ASW morphology heavily depends upon both surface temperature and deposition angle, ASW films grown at 125 K are expected to be insensitive to deposition method,[49] and thus all ice films studied here are consistent. Consequently, A and W are held constant in these fits to compare the projectiles within this framework, given their size does not prevent their embedding; they are all smaller than SF_6, the largest projectile we have investigated that did not embed at any energy examined.[28] The fits were performed with A held constant at 0.001 and W constrained between 1 and 2 eV for the case of CO_2 due to our data sampling only the low-energy region of the curve. The curves in Figure 4b clearly show that, over the examined energy range, the embedding probability of CO_2 (the projectile with the lowest mass) is significantly lower than that of the heavy CF_4 and Xe projectiles. Importantly, under this treatment, the *energetic* barrier values (E_0) for the Xe, CF_4, and CO_2 projectiles all yield nearly identical values for the barrier in terms of the *momentum*. Illustrated in Figure 5, the embedding probability is plotted against the incident translational momentum for all data collected by our group, and the complete momentum space sampled appears to trace a single curve. This is the first compelling empirical evidence in support of our prior conclusion that embedding efficacy is shaped by the incident translational momentum of a projectile upon collision with ice.[28]

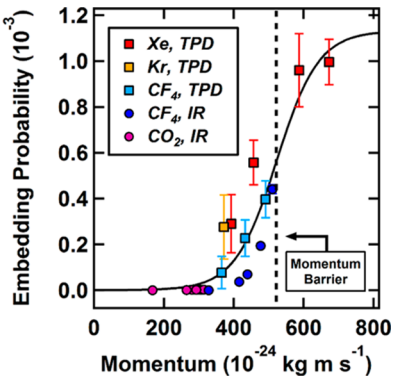

Figure 5. Accounting for the mass of each projectile yields a singular value for the barrier in terms of momentum. A plot of all amassed embedding data traces a unified barrier model across the sampled momentum space.

Open questions remain regarding the inherent differences in embedding efficacy involving ASW versus CI films. Ice films possess remarkable resilience to bombardment by high-energy projectiles via rapid energy dissipation,[41] and facile momentum transfer between projectiles and the recoiling ice matrix clearly leads to observable trapping at elevated temperatures relative to the desorption temperature of the projectiles, but perhaps *only* if the projectile drives deep enough into the ice film upon impact. Although possible that the local geometry encountered by a projectile is different between the two structures, factors affecting a projectile's persistence (i.e., extent of momentum transfer, mobility within the ice, cohesion of the surrounding ice lattice) after penetration are likely important, perhaps the most important, considerations; a higher persistence in ASW could possibly be linked to its ability to structurally accommodate the solute given its structural similarities with liquid water.[72−74] Though future theoretical work on this system is planned, support for this hypothesis comes in the form of prior molecular dynamics simulations of hyperthermal Xe collisions with hexagonal ice, where Xe atoms with high incident translational energy and trajectories primarily closer to normal incidence relative to the surface penetrated the vacuum−solid interface to greater depths, residing within the first one to four layers at the vacuum−solid interface and exhibiting low desorption probability at long ice residence time.[25,27]

■ CONCLUSION

Utilizing time-resolved *in situ* RAIRS we have conducted the first study of hyperthermal CO_2 capture by ASW under UHV conditions. These measurements were done at a temperature below but approaching its crystallization point. CO_2 is observed to directly embed underneath the vacuum−film interface and become trapped in the ice matrix at a much higher temperature than that allowed by thermal accretion, rapidly diffusing to form aggregates with primarily rod-like geometries, as suggested by the distinct spectroscopic signature observed. Application of a classical model treating the entrance of CO_2 and other gaseous projectiles into the ice as an activated process provides empirical evidence that projectile momentum is a general defining factor for embedding probability, provided that the projectile is not too large. Molecular dynamics simulations of the CO_2/H_2O interaction presented here would be a fruitful future endeavor and could provide further insight into the embedding of gaseous molecules with strong electrostatic interactions. Additionally, examination of embedding efficacies over a wider range of surface temperatures may better define the relationship between embedding probability and an embedded projectile's persistence in terms of its mobility within an amorphous ice film; we plan to pursue this route with the future construction of instrumentation capable of achieving significantly lower ice temperatures.

The results produced herein host significance in applications pertaining to the measurement and accurate modeling of gaseous accretion by ices, both terrestrial and extraterrestrial; relevant areas of interest include comet and planetesimal formation in the interstellar medium, gas capture related to global energy and climate issues, and the icing of aircraft in high velocity gas flows. A complete account of ice modification by gases is bolstered by recognition of embedding as a pathway for the uptake of gases by water ice at temperatures that would otherwise thermodynamically prohibit surface adsorption.

■ AUTHOR INFORMATION

Corresponding Author

*S. J. Sibener. E-mail: s-sibener@uchicago.edu.

DOI: 10.1021/acs.jpca.5b06287
J. Phys. Chem. A 2015, 119, 12238−12244

Author Contributions

†These authors contributed equally to this work, listed alphabetically

Notes

The authors declare no competing financial interest.

■ ACKNOWLEDGMENTS

This work was supported by the Air Force Office of Scientific Research, Grant No. FA9550-10-1-0219. Trace gas detection and environmental effects aspects of this work were sponsored by the Defense Threat Reduction Agency (DTRA) under Grant HDTRA1-11-1-0001. It is also a pleasure to acknowledge support from the University of Chicago Water Research Initiative. Infrastructure support from the NSF-Materials Research Science and Engineering Center at the University of Chicago, Grant No. NSF-DMR-14-20709, is also gratefully acknowledged.

■ REFERENCES

(1) Sill, G. T.; Wilkening, L. Ice Clathrate as a Possible Source of the Atmospheres of the Terrestrial Planets. *Icarus* **1978**, *33*, 13−27.

(2) Owen, T.; Bar-Nun, A. Comets, Impacts, and Atmospheres. *Icarus* **1995**, *116*, 215−226.

(3) Dauphas, N. The Dual Origin of the Terrestrial Atmosphere. *Icarus* **2003**, *165*, 326−339.

(4) Owen, T. The Contributions of Comets to Planets, Atmospheres, and Life: Insights from Cassini-Huygens, Galileo, Giotto, and Inner Planet Missions. *Space Sci. Rev.* **2008**, *138*, 301−316.

(5) Notesco, G.; Bar-Nun, A.; Owen, T. Gas Trapping in Water Ice at Very Low Deposition Rates and Implications for Comets. *Icarus* **2003**, *162*, 183−189.

(6) Yokoichi, R.; Marboeuf, U.; Quirico, E.; Schmitt, B. Pressure Dependent Trace Gas Trapping in Amorphous Water Ice at 77 K: Implications for Determining Conditions of Comet Formation. *Icarus* **2012**, *218*, 760−770.

(7) Burke, D. J.; Brown, W. A. Ice in Space: Surface Science Investigations of the Thermal Desorption of Model Interstellar Ices on Dust Grain Surface Analogs. *Phys. Chem. Chem. Phys.* **2010**, *12*, 5947−5969.

(8) Ehrenfreund, P.; Charnley, S. B. Organic Molecules in the Interstellar Medium, Comets, and Meteorites: A Voyage from Dark Clouds to the Early Earth. *Annu. Rev. Astron. Astrophys.* **2000**, *38*, 427−483.

(9) Gudipati, M. S.; Allamandola, L. J. Facile Generation and Storage of Polycyclic Aromatic Hydrocarbon Ions in Astrophysical Ices. *Astrophys. J.* **2003**, *596*, L195−L198.

(10) Nuevo, M.; Bredehöft, J. H.; Meierhenrich, U. J.; d'Hendecourt, L.; Thiemann, W. H.-P. Urea, Glycolic Acid, and Glycerol in an Organic Residue Produced by Ultraviolet Irradiation of Interstellar/Pre-Cometary Ice Analogs. *Astrobiology* **2010**, *10*, 245−256.

(11) Barks, H. L.; Buckley, R.; Grieves, G. A.; Mauro, E. D.; Hud, N. V.; Orlando, T. M. Guanine, Adenine, and Hypoxanthine Production in UV-Irradiated Formamide Solutions: Relaxation of the Requirements for Prebiotic Purine Nucleobase Formation. *ChemBioChem* **2010**, *11*, 1240−1243.

(12) Congiu, E.; Chaabouni, H.; Laffon, C.; Parent, P.; Baouche, S.; Dulieu, F. Efficient Surface Formation Route of Interstellar Hydroxylamine through NO Hydrogenation. I. The Submonolayer Regime on Interstellar Relevant Substrates. *J. Chem. Phys.* **2012**, *137*, 054713.

(13) Kaiser, R. I.; Maity, S.; Jones, B. M. Synthesis of Prebiotic Glycerol in Interstellar Ices. *Angew. Chem., Int. Ed.* **2015**, *54*, 195−200.

(14) de Marcellus, P.; Meinert, C.; Myrgorodska, I.; Nahon, L.; Buhse, T.; d'Hendecourt, L. L. S.; Meierhenrich, U. J. Aldehydes and Sugars from Evolved Precometary Ice Analogs: Importance of Ices in Astrochemical and Prebiotic Evolution. *Proc. Natl. Acad. Sci. U. S. A.* **2015**, *112*, 965−970.

(15) MacDonald, G. J. Role of Methane Clathrates in Past and Future Climates. *Clim. Change* **1990**, *16*, 247−281.

(16) Makogon, Y. F.; Holditch, S. F.; Makogon, T. Y. Natural Gas-Hydrates - A Potential Energy Source for the 21st Century. *J. Pet. Sci. Eng.* **2007**, *56*, 14−31.

(17) Schüth, F. Technology: Hydrogen and Hydrates. *Nature* **2005**, *434*, 712−713.

(18) Veluswarmy, H. P.; Kumar, R.; Linga, P. Hydrogen Storage in Clathrate Hydrates: Current State of the Art and Future Directions. *Appl. Energy* **2014**, *122*, 112−132.

(19) Aaron, D.; Touris, C. Separation of CO_2 from Flue Gas: A Review. *Sep. Sci. Technol.* **2005**, *40*, 321−348.

(20) Linga, P.; Kumar, R.; Lee, J. D.; Ripmeester, J.; Englezos, P. A New Apparatus to Enhance the Rate of Gas Hydrate Formation: Application to Capture of Carbon Dioxide. *Int. J. Greenhouse Gas Control* **2010**, *4*, 630−637.

(21) d'Hendecourt, L. B.; de Muizon, M. J. The Discovery of Interstellar Carbon Dioxide. *Astron. Astrophys.* **1989**, *223*, L3−L8.

(22) Gibb, E. L.; Whittet, D. C. B.; Schutte, W. A.; Boogert, A. C. A.; Chiar, J. E.; Ehrenfreund, P.; Gerakines, P. A.; Keane, J. V.; Tielens, A. G. G. M.; van Dishoeck, E. F.; Kerkhof, O. An Inventory of Interstellar Ices toward the Embedded Protostar W33A. *Astrophys. J.* **2000**, *536*, 347−356.

(23) Martínez-Botí, M. A.; Foster, G. L.; Chalk, T. B.; Rohling, E. J.; Sexton, P. F.; Lunt, D. J.; Pancost, R. D.; Badger, M. P. S.; Schmidt, D. N. Plio-Pleistocene Climate Sensitivity Evaluated Using High-Resolution CO_2 Records. *Nature* **2015**, *518*, 49−54.

(24) Martínez-Botí, M. A.; Marino, G.; Foster, G. L.; Ziveri, P.; Henehan, M. J.; Rae, J. W. B.; Mortyn, P. G.; Vance, D. Boron Isotope Evidence for Oceanic Carbon Dioxide Leakage during the Last Deglaciation. *Nature* **2015**, *518*, 219−222.

(25) Gibson, K. D.; Killelea, D. R.; Yuan, H.; Becker, J. S.; Pratihar, S.; Manikandan, P.; Kohale, S. C.; Hase, W. L.; Sibener, S. J. Scattering of High-Incident-Energy Kr and Xe from Ice: Evidence that a Major Channel Involves Penetration into the Bulk. *J. Phys. Chem. C* **2012**, *116*, 14264−14273.

(26) Gibson, K. D.; Killelea, D. R.; Becker, J. S.; Yuan, H.; Sibener, S. J. Energetic Ballistic Deposition of Volatile Gases into Ice. *Chem. Phys. Lett.* **2012**, *531*, 18−21.

(27) Pratihar, S.; Kohale, S. C.; Yang, L.; Manikandan, P.; Gibson, K. D.; Killelea, D. R.; Yuan, H.; Sibener, S. J.; Hase, W. L. Chemical Dynamics Simulations of High Energy Xenon Atom Collisions with the (0001) Surface of Hexagonal Ice. *J. Phys. Chem. C* **2013**, *117*, 2183−2193.

(28) Gibson, K. D.; Langlois, G. G.; Li, W.; Killelea, D. R.; Sibener, S. J. Molecular Interactions with Ice: Molecular Embedding, Adsorption, Detection, and Release. *J. Chem. Phys.* **2014**, *141*, 18C514.

(29) Ocampo, J.; Klinger, J. Adsorption of N_2 and CO_2 on Ice. *J. Colloid Interface Sci.* **1982**, *86*, 377−383.

(30) Bar-Nun, A.; Dror, J.; Kochavi, E.; Laufer, D. Amorphous Water Ice and its Ability to Trap Gases. *Phys. Rev. B: Condens. Matter Mater. Phys.* **1987**, *35*, 2427−2435.

(31) Notesco, G.; Bar-Nun, A. Trapping of Methanol, Hydrogen Cyanide, and *n*-Hexane in Water Ice, above its Transition Temperature to the Crystalline Form. *Icarus* **1997**, *126*, 336−341.

(32) Collings, M. P.; Anderson, M. A.; Chen, R.; Dever, J. W.; Viti, S.; Williams, D. A.; McCoustra, M. R. S. A Laboratory Survey of the Thermal Desorption of Astrophysically Relevant Molecules. *Mon. Not. R. Astron. Soc.* **2004**, *354*, 1133−1140.

(33) Kumi, G.; Malyk, S.; Hawkins, S.; Reisler, H.; Wittig, C. Amorphous Solid Water Films: Transport and Guest-Host Interactions with CO_2 and N_2O Dopants. *J. Phys. Chem. A* **2006**, *110*, 2097−2105.

(34) Hood, L. L. Thermal Processing of Chondrule Precursors in Planetesimal Bow Shocks. *Meteorit. Planet. Sci.* **1998**, *33*, 97−107.

(35) Joslin, R. D. Aircraft Laminar Flow Control. *Annu. Rev. Fluid Mech.* **1998**, *30*, 1−29.

(36) Cebeci, T.; Kafyeke, F. Aircraft Icing. *Annu. Rev. Fluid Mech.* **2003**, *35*, 11−21.

DOI: 10.1021/acs.jpca.5b06287
J. Phys. Chem. A 2015, 119, 12238−12244

(37) Gibson, K. D.; Killelea, D. R.; Yuan, H.; Becker, J. S.; Sibener, S. J. Determination of the Sticking Coefficient and Scattering Dynamics of Water on Ice Using Molecular Beam Techniques. *J. Chem. Phys.* **2011**, *134*, 034703.
(38) Pirug, G.; Bonzel, H. P. UHV Simulation of the Electrochemical Double Layer: Adsorption of $HClO_4/H_2O$ on Au(111). *Surf. Sci.* **1998**, *405*, 87−103.
(39) Henderson, M. A. The Interaction of Water with Solid Surfaces: Fundamental Aspects Revisited. *Surf. Sci. Rep.* **2002**, *46*, 1−308.
(40) Hodgson, A.; Haq, S. Water Adsorption and the Wetting of Metal Surfaces. *Surf. Sci. Rep.* **2009**, *64*, 381−451.
(41) Killelea, D. R.; Gibson, K. D.; Yuan, H.; Becker, J. S.; Sibener, S. J. Dynamics of the Sputtering of Water from Ice Films by Collisions with Energetic Xenon Atoms. *J. Chem. Phys.* **2012**, *136*, 144705.
(42) Tingey, G. L. Kinetics of the Water-Gas Equilibrium Reaction. I. The Reaction of Carbon Dioxide with Hydrogen. *J. Phys. Chem.* **1966**, *70*, 1406−1412.
(43) Shebaro, L.; Bhalotra, S. R.; Herschbach, D. Molecular Beam Chemistry: Formation of Benzene and Other Higher Hydrocarbons from Small Alkanes and Alkenes in a Catalytic Supersonic Nozzle. *J. Phys. Chem. A* **1997**, *101*, 6775−6780.
(44) Itikawa, Y. Cross Sections for Electron Collisions with Carbon Dioxide. *J. Phys. Chem. Ref. Data* **2002**, *31*, 749−767.
(45) Itikawa, Y. Cross Sections for Electron Collisions with Nitrogen Molecules. *J. Phys. Chem. Ref. Data* **2006**, *35*, 31−53.
(46) Falk, M. Amorphous Solid Carbon Dioxide. *J. Chem. Phys.* **1987**, *86*, 560−564.
(47) Gálvez, O.; Ortega, I. K.; Maté, B.; Moreno, M. A.; Martín-Llorente, B.; Herrero, V. J.; Escribano, R.; Gutiérrez, P. J. A Study of the Interaction of CO_2 with Water Ice. *Astron. Astrophys.* **2007**, *472*, 691−698.
(48) Bernstein, M. P.; Cruikshank, D. P.; Sanford, S. A. Near-Infrared Laboratory Spectra of Solid H_2O/CO_2 and CH_3OH/CO_2 Ice Mixtures. *Icarus* **2005**, *179*, 527−534.
(49) Kimmel, G. A.; Stevenson, K. P.; Dohnálek, Z.; Smith, R. S.; Kay, B. D. Control of Amorphous Solid Water Morphology using Molecular Beams. I. Experimental Results. *J. Chem. Phys.* **2001**, *114*, 5284−5294.
(50) Hodyss, R.; Johnson, P. V.; Orzechowska, G. E.; Goguen, J. D.; Kanik, I. Carbon Dioxide Segregation in 1:4 and 1:9 CO_2:H_2O Ices. *Icarus* **2008**, *194*, 836−842.
(51) Barnes, J. A.; Gough, T. E. Fourier Transform Infrared Spectroscopy of Molecular Clusters: The Structure and Internal Mobility of Clustered Carbon Dioxide. *J. Chem. Phys.* **1987**, *86*, 6012−6017.
(52) Ewing, G. E.; Sheng, D. T. Infrared Spectroscopy of CO_2 Ultrafine Particles. *J. Phys. Chem.* **1988**, *92*, 4063−4066.
(53) Fleyfel, F.; Devlin, J. P. FT-IR Spectra of CO_2 Clusters. *J. Phys. Chem.* **1989**, *93*, 7292−7294.
(54) Signorell, R.; Kunzmann, M. K. Isotope Effects on Vibrational Excitons in Carbon Dioxide Particles. *Chem. Phys. Lett.* **2003**, *371*, 260−266.
(55) Bonnamy, A.; Georges, R.; Hugo, E.; Signorell, R. IR Signature of $(CO_2)_N$ Clusters: Size, Shape, and Structural Effects. *Phys. Chem. Chem. Phys.* **2005**, *7*, 963−969.
(56) Jones, L. H.; Swanson, B. I. Transverse Optical to Longitudinal Optical Splitting and Dipole Moment Derivatives from Infrared Spectra of Thin Films of Molecular Solids. *J. Phys. Chem.* **1991**, *95*, 2701−2707.
(57) Ovchinnikov, M. A.; Wight, C. A. Inhomogeneous Broadening of Infrared and Raman Spectral Bands of Amorphous and Polycrystalline Thin Films. *J. Chem. Phys.* **1993**, *99*, 3374−3379.
(58) Taraschewski, M.; Cammenga, H. K.; Tuckermann, R.; Bauerecker, S. FTIR Study of CO_2 and H_2O/CO_2 Nanoparticles and Their Temporal Evolution at 80 K. *J. Phys. Chem. A* **2005**, *109*, 3337−3343.
(59) Winkler, M.; Harnes, J.; Børve, K. J. Structure of Neutral Nanosized Clusters Produced by Coexpansion of CF_4 and CH_4. *J. Phys. Chem. A* **2011**, *115*, 13259−13268.
(60) Tsuzuki, S.; Uchimaru, T.; Mikami, M.; Urata, S. Magnitude and Orientation Dependence of Intermolecular Interaction between Perfluoroalkanes: High Level *ab initio* Calculations of CF_4 and C_2F_6 dimers. *J. Chem. Phys.* **2002**, *116*, 3309−3315.
(61) Mahlanen, R.; Jalkanen, J.-P.; Pakkanen, T. A. Potential Energy Surfaces of CF_4, CCl_4, and CBr_4 Dimers. *Chem. Phys.* **2005**, *313*, 271−277.
(62) Caminati, W.; Maris, A.; Dell'Erba, A.; Favero, P. G. Dynamical Behavior and Dipole-Dipole Interactions of Tetrafluoromethane-Water. *Angew. Chem., Int. Ed.* **2006**, *45*, 6711−6714.
(63) Sandford, S. A.; Allamandola, L. J. The Physical and Infrared Spectral Properties of CO_2 in Astrophysical Ice Analogs. *Astrophys. J.* **1990**, *355*, 357−372.
(64) Escribano, R. M.; Muñoz Caro, G. M.; Cruz-Diaz, G. A.; Rodríguez-Lazcano, Y.; Maté, B. Crystallization of CO_2 Ice and the Absence of Amorphous CO_2 Ice in Space. *Proc. Natl. Acad. Sci. U. S. A.* **2013**, *110*, 12899−12904.
(65) Ehrenfreund, P.; Boogert, A. C. A.; Gerakines, P. A.; Tielens, A. G. G. M.; van Dishoeck, E. F. Infrared Spectroscopy of Interstellar Apolar Ice Analogs. *Astron. Astrophys.* **1997**, *328*, 649−669.
(66) Buch, V.; Delzeit, L.; Blackledge, C.; Devlin, J. P. Structure of the Ice Nanocrystal Surface from Simulated versus Experimental Spectra of Adsorbed CF_4. *J. Phys. Chem.* **1996**, *100*, 3732−3744.
(67) Devlin, J. P.; Buch, V. Vibrational Spectroscopy and Modeling of the Surface and Subsurface of Ice and of Ice-Adsorbate Interactions. *J. Phys. Chem. B* **1997**, *101*, 6095−6098.
(68) *CRC Handbook of Chemistry and Physics*, 89th ed.; CRC Press: Boca Raton, FL, 2008−2009; pp 6−36.
(69) Lennard-Jones, J. E. Processes of Adsorption and Diffusion on Solid Surfaces. *Trans. Faraday Soc.* **1932**, *28*, 333−359.
(70) Balooch, M.; Cardillo, M. J.; Miller, D. R.; Stickney, R. D. Molecular Beam Study of the Apparent Activation Barrier associated with Adsorption and Desorption of Hydrogen on Copper. *Surf. Sci.* **1974**, *46*, 358−392.
(71) Harris, J. On Vibrationally-Assisted Dissociation of H_2 at Metal Surfaces. *Surf. Sci.* **1989**, *221*, 335−345.
(72) Smith, R. S.; Dohnálek, Z.; Kimmel, G. A.; Stevenson, K. P.; Kay, B. D. The Self-Diffusivity of Amorphous Solid Water near 150 K. *Chem. Phys.* **2000**, *258*, 291−305.
(73) Angell, C. A. Amorphous Water. *Annu. Rev. Phys. Chem.* **2004**, *55*, 559−583.
(74) Shalit, A.; Perakis, F.; Hamm, P. Two-Dimensional Infrared Spectroscopy of Isotope-Diluted Low Density Amorphous Ice. *J. Phys. Chem. B* **2013**, *117*, 15512−15518.

DOI: 10.1021/acs.jpca.5b06287
J. Phys. Chem. A 2015, 119, 12238−12244